Higher Order Compact Scheme for Time Deforming Domains

Shuvam Sen
Department of Mathematical Sciences
Tezpur University, India

Tony W. H. Sheu
Department of Engineering Science & Ocean Engineering
National Taiwan University, Taipei, Taiwan

Taiwan-India Joint Conference
– Recent Progress on Flow Simulation and Stability Analysis
National Taiwan University, Taipei, Taiwan
March 17, 2019

Outline

Background

- In CFD, large-eddy simulation, aeroacoustics, fluid-structure interaction are of great interest.
- Higher order compact (HOC) schemes represent an attractive choice for reducing severe computational requirements.
- For incompressible flow HOC has been used in conjunction with simple domains discretized by static Cartesian meshes.
- Practically relevant problems require curvilinear time-varying meshes with limited smoothness.

Objectives

1. Extend higher order compact discretization to convection-diffusion equation in curvilinear deforming meshes.
2. To solve incompressible Navier-Stokes (N-S) equations in time varying domains.
3. Study impact of not so smooth body fitted grids in simulating incompressible flow using non-conservative form of N-S equations.
4. To ensure advantages of higher order approach over existing lower order schemes.

Moving Domain

- For geometries undergoing dynamic movement or deformation, a method for accommodating boundary movements is needed before numerical discretization of flow equations.

- Methods available:
  1. Immersed boundary method,
  2. Flow domain remeshing method,
  3. Mesh displacement method.

Methods

- Immersed boundary method:
  - Advantage- does not require the grid to conform to the shape of geometric boundaries.
  - Disadvantage- not clear if it is possible to achieve the desired high order of accuracy.
- Flow domain remeshing method:
  - Advantage- no constraint on boundary movement as finite element discretization can be used for each newly generated mesh.
  - Disadvantage- computationally expensive, interpolation between successive meshes may not maintain accuracy.
- Mesh displacement method:
  - Advantage- preserve the high order of accuracy of the underlying scheme.
  - Disadvantage- till now limited to simple boundary movement problems.

Challenges

- Continuous boundary movement requires dynamic coordinate transformation between physical and computational domains.
- Mapping needs to be constructed at every time step.
- Motion of the grid points introduces dynamic information, needs to be properly accounted.

Discretization of Governing Equation

- Higher order compact discretization of Navier-Stokes system, cast in strong conservation form on general time-dependent curvilinear coordinate, was introduced by Visbal & Gaitonde (2002 [1]).
- Authors in [1] approximate first derivative only and employ repeated application of the same to compute viscous term.
- A spatially fourth order and temporally second order compact finite difference scheme for generalized convection-diffusion equation was proposed by Sen (2013 [2], 2016 [3]).

Geometric Conservation Law (GCL)

First coined by Thomas and Lombard (1979 [4]).

Integral form of GCL

$$\frac{d}{dt}\int_{cell} dv = \int_{\partial cell} \overrightarrow{q}.\hat{n}ds$$

$\overrightarrow{q}$ mesh velocity.

Differential form of GCL in 2D

$$(\xi_x J)_\xi + (\eta_x J)_\eta = 0,$$
$$(\xi_y J)_\xi + (\eta_y J)_\eta = 0,$$
$$(J)_\tau - (J_1)_\xi - (J_2)_\eta = 0,$$

J, J_1, J_2 are spatial and temporal metrics.

Understanding GCL in 1D

Consider 1D convection-diffusion equation

Non-conservative form

$$\frac{\partial \phi}{\partial t} - a\frac{\partial^2 \phi}{\partial x^2} + c\frac{\partial \phi}{\partial x} = 0.$$

Conservative form

$$\frac{\partial \phi}{\partial t} - \frac{\partial}{\partial x}\left(a\frac{\partial \phi}{\partial x}\right) + \frac{\partial}{\partial x}\left(c\phi\right) = 0.$$

For a dynamically deforming mesh in 1D

$$x = x(\xi, \tau), \quad \tau = t.$$

Understanding GCL in 1D

Thus using chain rule

$$(.)_t = \xi_t (.)_\xi + (.)_\tau, \quad (.)_x = \xi_x (.)_\xi \ \text{ with } \ J = x_\xi, \ \ J_1 = x_\tau.$$

Non-conservative form

$$\frac{\partial \phi}{\partial \tau} - \frac{a}{J^2}\frac{\partial^2 \phi}{\partial \xi^2} + \left[\frac{1}{J}(-J_1 + c) + \frac{a}{J^3} J_\xi\right] \frac{\partial \phi}{\partial \xi} = 0.$$

Conservative form

$$\frac{\partial}{\partial \tau}(J\phi) - \frac{\partial}{\partial \xi}\left(aJ\frac{\partial \phi}{\partial \xi}\right) + \frac{\partial}{\partial \xi}\left((-J_1 + c)\phi\right) = \phi\left[(J)_\tau - (J_1)_\xi\right].$$

Metric Evaluation

- Satisfaction of GCL is **essential** for simulation using conservative form.
- May not hamper computation carried out with non-conservative form.
- What about free stream preservation?
- Nevertheless computation of temporal and spatial grid metrics upto the respective desired levels of accuracy is imperative.

Outline

Governing Equation

For transport variable $\phi(x, y, t)$ with spatial variables (x, y) defined over an arbitrary domain $D \subset \mathbb{R}^2$ the convection-diffusion equation is

$$\frac{\partial \phi}{\partial t} - a(x, y, t)\left(\frac{\partial^2 \phi}{\partial x^2} + \frac{\partial^2 \phi}{\partial y^2}\right) + c_1(x, y, t)\frac{\partial \phi}{\partial x} + c_2(x, y, t)\frac{\partial \phi}{\partial y} = s(x, y, t), \tag{1}$$

$(x, y, t) \in D \times (0, T]$ with the initial condition

$$\phi(x, y, 0) = \phi_0(x, y), \qquad (x, y) \in D \tag{2}$$

and boundary condition

$$b_1(x, y, t)\phi + b_2(x, y, t)\frac{\partial \phi}{\partial \boldsymbol{n}} = g(x, y, t), \qquad (x, y) \in \partial D, \;\; t \in (0, T]. \tag{3}$$

Here $a(x, y, t) > 0$ and n is unit boundary normal vector.

Time Varying Transformation

We introduce the following time varying body fitted coordinate transformation

$$x = x(\xi, \eta, \tau), \quad y = y(\xi, \eta, \tau), \quad t = \tau \tag{4}$$

from non-dimensionalized Cartesian coordinate system to the curvilinear coordinate system, where

Jacobian $J = \dfrac{\partial(x,y)}{\partial(\xi,\eta)} \neq 0$ and $J_1 = \dfrac{\partial(x,y)}{\partial(\tau,\eta)}$, $J_2 = \dfrac{\partial(x,y)}{\partial(\xi,\tau)}$.

Transformed Equation

In the computational plane the equation reduces to

$$\frac{\partial \phi}{\partial \tau} - \alpha_1(\xi,\eta,\tau)\frac{\partial^2 \phi}{\partial \xi^2} - \beta(\xi,\eta,\tau)\frac{\partial^2 \phi}{\partial \xi \partial \eta} - \alpha_2(\xi,\eta,\tau)\frac{\partial^2 \phi}{\partial \eta^2}$$
$$+\chi_1(\xi,\eta,\tau)\frac{\partial \phi}{\partial \xi} + \chi_2(\xi,\eta,\tau)\frac{\partial \phi}{\partial \eta} = s(\xi,\eta,\tau), \tag{5}$$

$(\xi,\eta,\tau) \in \Omega \times (0,T]$ with the initial condition

$$\phi(\xi,\eta,0) = \phi_0(\xi,\eta), \qquad (\xi,\eta) \in \Omega \tag{6}$$

and boundary condition

$$\vartheta_1(\xi,\eta,\tau)\phi + \vartheta_2(\xi,\eta,\tau)\frac{\partial \phi}{\partial \boldsymbol{\nu}} = g(\xi,\eta,\tau), \qquad (\xi,\eta) \in \partial\Omega, \;\; \tau \in (0,T]. \tag{7}$$

Eq. (5) possesses positive definiteness of the diffusion matrix *i.e.* $\alpha_1 > 0$, $\alpha_2 > 0$, $|\beta|^2 \leq 4\alpha_1\alpha_2 \;\forall\; (\xi,\eta,\tau) \in \Omega \times (0,T]$.

Transformed Equation

$$
\begin{aligned}
\alpha_1 &= \frac{a}{J^2}(x_\eta^2 + y_\eta^2), \\
\alpha_2 &= \frac{a}{J^2}(x_\xi^2 + y_\xi^2), \\
\beta &= -\frac{2a}{J^2}(x_\xi x_\eta + y_\xi x_\eta), \\
\chi_1 &= \frac{1}{J}(-J_1 + cy_\eta - dx_\eta) - \frac{a}{J^3}\Big(J_\eta(x_\xi x_\eta + y_\xi y_\eta) \\
&\quad -J_\xi(x_\eta^2 + y_\eta^2) + J(x_\eta x_{\xi\eta} + y_\eta y_{\xi\eta} - x_\xi x_{\eta\eta} - y_\xi y_{\eta\eta}\Big), \\
\chi_2 &= \frac{1}{J}(-J_2 - cy_\xi + dx_\xi) - \frac{a}{J^3}\Big(J_\xi(x_\xi x_\eta + y_\xi y_\eta) \\
&\quad -J_\eta(x_\xi^2 + y_\xi^2) + J(x_\xi x_{\xi\eta} + y_\xi y_{\xi\eta} - x_\eta x_{\xi\xi} - y_\eta y_{\xi\xi}\Big).
\end{aligned}
$$

Transformed Equation

Introducing partial differential operator $[A]$

$$[A] \equiv [-\alpha_1 \partial_{\xi\xi} - \beta \partial_{\xi\eta} - \alpha_2 \partial_{\eta\eta} + \chi_1 \partial_\xi + \chi_2 \partial_\eta], \tag{8}$$

equation (5) reduces to:

$$\begin{cases} \partial_t \phi(\xi,\eta,\tau) + A\phi(\xi,\eta,\tau) = s(\xi,\eta,\tau), & (\xi,\eta,\tau) \in \Omega \times (0,T] \\ \phi(\xi,\eta,0) = \phi_0(\xi,\eta), & (\xi,\eta) \in \Omega \\ \vartheta_1(\xi,\eta,\tau)\phi + \vartheta_2(\xi,\eta,\tau)\partial_{\boldsymbol{\nu}}\phi = g(\xi,\eta,\tau), & (\xi,\eta) \in \partial\Omega,\ \tau \in (0,T] \end{cases} \tag{9}$$

Discretization I

Semi-discrete $O(h^4, k^4, h^2k^2)$ approximation of the governing Eq. (9) on a nine point stencil is

$$\partial_t \phi_{i,j} + A_{h,k}\phi_{i,j} = s_{i,j}, \tag{10}$$

where the discrete operator $A_{h,k}$ is defined as [3]

$$\begin{aligned} A_{h,k}\phi_{i,j} &= (-2\alpha_{1_{i,j}}\delta_\xi^2 - 2\alpha_{2_{i,j}}\delta_\eta^2 + \beta_{i,j}\delta_\xi\delta_\eta)\phi_{i,j} \\ &+(\alpha_{1_{i,j}}\delta_\xi - \beta_{i,j}\delta_\eta + \chi_{1_{i,j}})\phi_{\xi_{i,j}} + (\alpha_{2_{i,j}}\delta_\eta - \beta_{i,j}\delta_\xi + \chi_{2_{i,j}})\phi_{\eta_{i,j}}. \end{aligned} \tag{11}$$

h and k are uniform step sizes along ξ and η directions respectively.

Discretization II

Compatible fourth order approximations for space derivatives are accomplished by using Padé approximations.

$$\left(I + \frac{h^2}{6}\delta_\xi^2\right)\phi_{\xi_{i,j}} = \delta_\xi \phi_{i,j}, \tag{12}$$

and

$$\left(I + \frac{k^2}{6}\delta_\eta^2\right)\phi_{\eta_{i,j}} = \delta_\eta \phi_{i,j}. \tag{13}$$

Implicit time discretization

Temporal discretization done using 2^{nd} order Crank-Nicolson method. Fully discrete scheme for grid point (i,j) at time level (n) is

$$\left(1+\frac{\delta\tau}{2}A_{h,k}\right)\phi_{i,j}^{(n+1)}=\left(1-\frac{\delta\tau}{2}A_{h,k}\right)\phi_{i,j}^{(n)}+\frac{\delta\tau}{2}\left(s_{i,j}^{(n+1)}+s_{i,j}^{(n)}\right). \quad (14)$$

Details of stability of this scheme can be found in [2]. On expansion

$$\begin{aligned}
&[1-\frac{\delta\tau}{2}(2\alpha_{1_{i,j}}^{(n+1)}\delta_\xi^2+2\alpha_{2_{i,j}}^{(n+1)}\delta_\eta^2-\beta_{i,j}^{(n+1)}\delta_\xi\delta_\eta)]\phi_{i,j}^{(n+1)}\\
&=[1+\frac{\delta\tau}{2}(2\alpha_{1_{i,j}}^{(n)}\delta_\xi^2+2\alpha_{2_{i,j}}^{(n)}\delta_\eta^2-\beta_{i,j}^{(n)}\delta_\xi\delta_\eta)]\phi_{i,j}^{(n)}\\
&-\frac{\delta\tau}{2}[(\alpha_{1_{i,j}}^{(n)}\delta_\xi-\beta_{i,j}^{(n)}\delta_\eta+\chi_{1_{i,j}}^{(n)})\phi_{\xi_{i,j}}^{(n)}+(\alpha_{2_{i,j}}^{(n)}\delta_\eta-\beta_{i,j}^{(n)}\delta_\xi+\chi_{2_{i,j}}^{(n)})\phi_{\eta_{i,j}}^{(n)}]\\
&+(\alpha_{1_{i,j}}^{(n+1)}\delta_\xi-\beta_{i,j}^{(n+1)}\delta_\eta+\chi_{1_{i,j}}^{(n+1)})\phi_{\xi_{i,j}}^{(n+1)}\\
&+(\alpha_{2_{i,j}}^{(n+1)}\delta_\eta-\beta_{i,j}^{(n+1)}\delta_\xi+\chi_{2_{i,j}}^{(n+1)})\phi_{\eta_{i,j}}^{(n+1)}-s_{i,j}^{(n)}-s_{i,j}^{(n+1)}].
\end{aligned}$$

Stencil

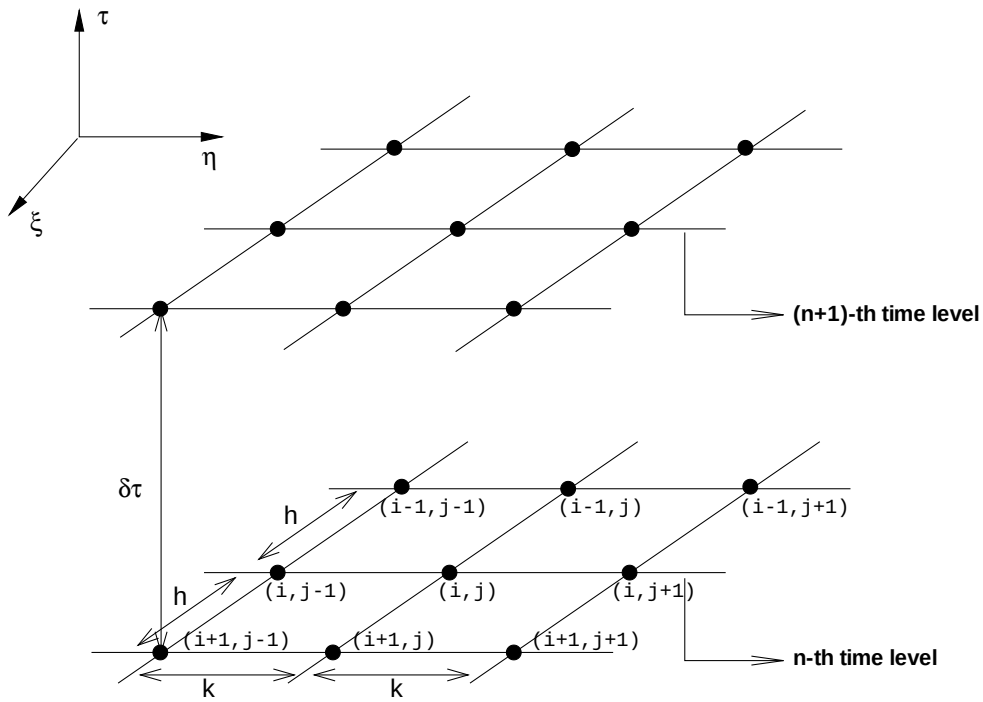

Figure 1: *Computational stencil: the used nodes are denoted by "•".*

Elliptic Equation

2D Elliptic equation of the form

$$-\left(\frac{\partial^2\phi}{\partial x^2}+\frac{\partial^2\phi}{\partial y^2}\right)=s(x,y,t) \tag{15}$$

in physical plane under transformation

$$x=x(\xi,\eta,\tau),\quad y=y(\xi,\eta,\tau),\quad t=\tau$$

reduces to

$$\begin{aligned}-\alpha_1(\xi,\eta,\tau)\frac{\partial^2\phi}{\partial\xi^2}-\beta(\xi,\eta,\tau)\frac{\partial^2\phi}{\partial\xi\partial\eta}-\alpha_2(\xi,\eta,\tau)\frac{\partial^2\phi}{\partial\eta^2}\\ +\chi_1(\xi,\eta,\tau)\frac{\partial\phi}{\partial\xi}+\chi_2(\xi,\eta,\tau)\frac{\partial\phi}{\partial\eta}=s(\xi,\eta,\tau),\end{aligned} \tag{16}$$

Discretized Elliptic Equation

$$\alpha_1 = \frac{1}{J^2}(x_\eta^2 + y_\eta^2), \quad \alpha_2 = \frac{1}{J^2}(x_\xi^2 + y_\xi^2), \quad \beta = -\frac{2}{J^2}(x_\xi x_\eta + y_\xi x_\eta),$$

$$\chi_1 = -\frac{1}{J^3}\Big(J_\eta(x_\xi x_\eta + y_\xi y_\eta) - J_\xi(x_\eta^2 + y_\eta^2) + J(x_\eta x_{\xi\eta} + y_\eta y_{\xi\eta} - x_\xi x_{\eta\eta} - y_\xi y_{\eta\eta}\Big),$$

$$\chi_2 = -\frac{1}{J^3}\Big(J_\xi(x_\xi x_\eta + y_\xi y_\eta) - J_\eta(x_\xi^2 + y_\xi^2) + J(x_\xi x_{\xi\eta} + y_\xi y_{\xi\eta} - x_\eta x_{\xi\xi} - y_\eta y_{\xi\xi}\Big).$$

The discrete form of the equation (16) is

$$\begin{aligned}&(-2\alpha_{1_{i,j}}\delta_\xi^2 - 2\alpha_{2_{i,j}}\delta_\eta^2 + \beta_{i,j}\delta_\xi\delta_\eta)\phi_{i,j} + (\alpha_{1_{i,j}}\delta_\xi - \beta_{i,j}\delta_\eta + \chi_{1_{i,j}})\phi_{\xi_{i,j}} \\ &+(\alpha_{2_{i,j}}\delta_\eta - \beta_{i,j}\delta_\xi + \chi_{2_{i,j}})\phi_{\eta_{i,j}} = s_{i,j}. \qquad (17)\end{aligned}$$

Grid Metrics

Spatial and temporal metrics are computed in three different fashions:

- Following newly developed symmetric-conservative metric evaluation procedure of Abe et al. [6, 7]. The procedure ensuring automatic satisfaction of GCL identities in 2D is given by,

$$\begin{aligned} J &= [(x_\xi y)_\eta - (x_\eta y)_\xi + (x y_\eta)_\xi - (x y_\xi)_\eta]/2, \\ J_1 &= [(x_\tau y)_\eta - (x_\eta y)_\tau + (x y_\eta)_\tau - (x y_\tau)_\eta]/2, \\ J_2 &= [(x_\xi y)_\tau - (x_\tau y)_\xi + (x y_\tau)_\xi - (x y_\xi)_\tau]/2. \end{aligned}$$

- Using compact stencil.
- Using wide non-compact stencil.

In all computations fourth order spatial and first order temporal accuracy is maintained.

Grid Movement

Grid movements are carried in either of the two different ways:

1. Using closed form expression.
2. Using Inverse Distance Weighting (IDW) interpolation.
   - Initialized by Witteveen & Bijl (2009 [8]) and Witteveen (2010 [9]).
   - Utilize reciprocal distance weighted sums of the boundary node displacements to the volume vertices.
   - The method was improved later by Luke et al. (2012 [10]).

Outline

Flow Decayed by Viscosity

A validation study is carried out by solving 2D N-S system

$$\frac{\partial \vec{q}}{\partial t} + (\vec{q}.\nabla)\vec{q} - \frac{1}{Re}\nabla^2\vec{q} = -\nabla p, \tag{18}$$

$$-\nabla^2 p = \nabla.[(\vec{q}.\nabla)\vec{q}], \tag{19}$$

with $\vec{q} = (-\cos x \sin y e^{\frac{-2t}{Re}}, \sin x \cos y e^{\frac{-2t}{Re}}), \quad p = -\frac{(\cos 2x + \cos 2y)}{4} e^{\frac{-4t}{Re}}.$
A wavy curvilinear time deforming grid [1] is generated using

$$\begin{aligned} x_{i,j} &= \xi_{\min} + h\left[i + A_x \sin(2\pi\varpi\tau) \times \sin\left(\frac{n_x \pi j k}{\eta_{\max} - \eta_{\min}}\right)\right], \\ y_{i,j} &= \eta_{\min} + k\left[j + A_y \sin(2\pi\varpi\tau) \times \sin\left(\frac{n_y \pi i h}{\xi_{\max} - \xi_{\min}}\right)\right]. \end{aligned} \tag{20}$$

We take $A_x = 1 = A_y$, $n_x = 6 = n_y$, $\varpi = 0.25$, $\xi_{\min} = 0 = \eta_{\min}$, $\xi_{\max} = \pi = \eta_{\max}$ and solve using a 61×61 grid with $\delta t = 0.0025$.

Flow Decayed by Viscosity

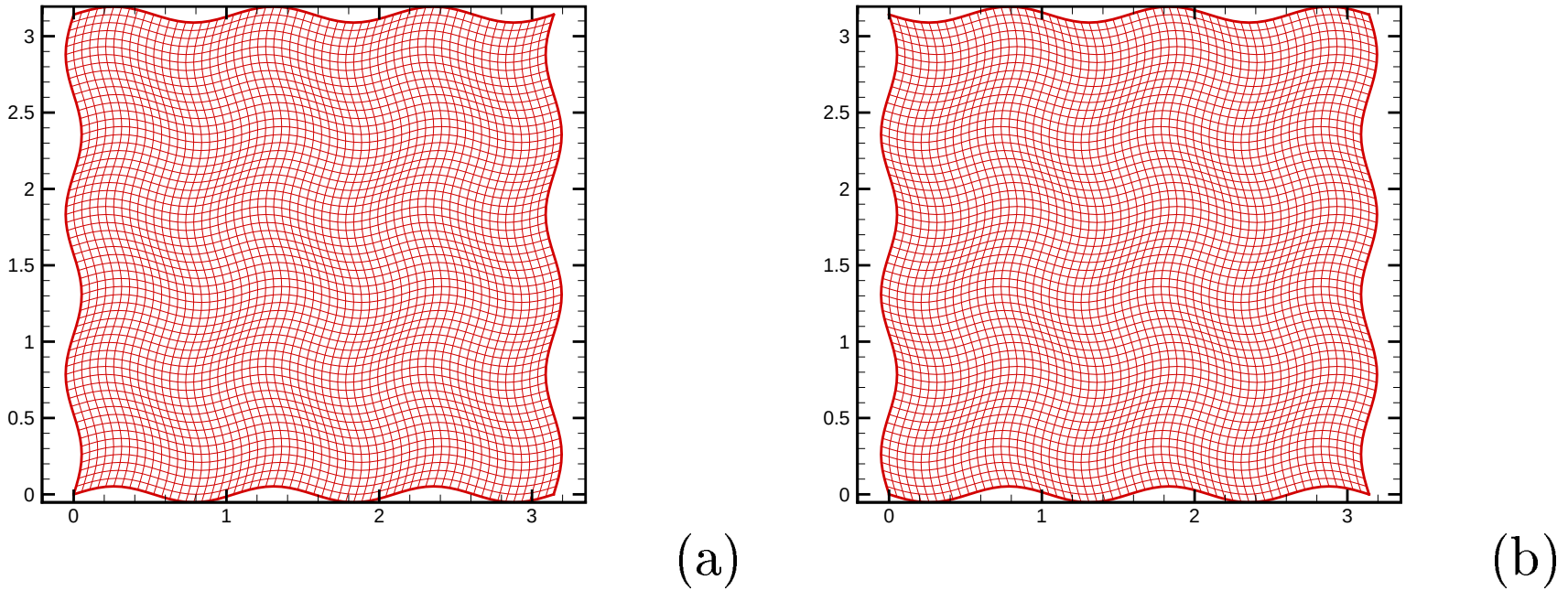

Figure 2: *Grid at time (a) $t = 1$, (b) $t = 3$.*

Flow Decayed by Viscosity

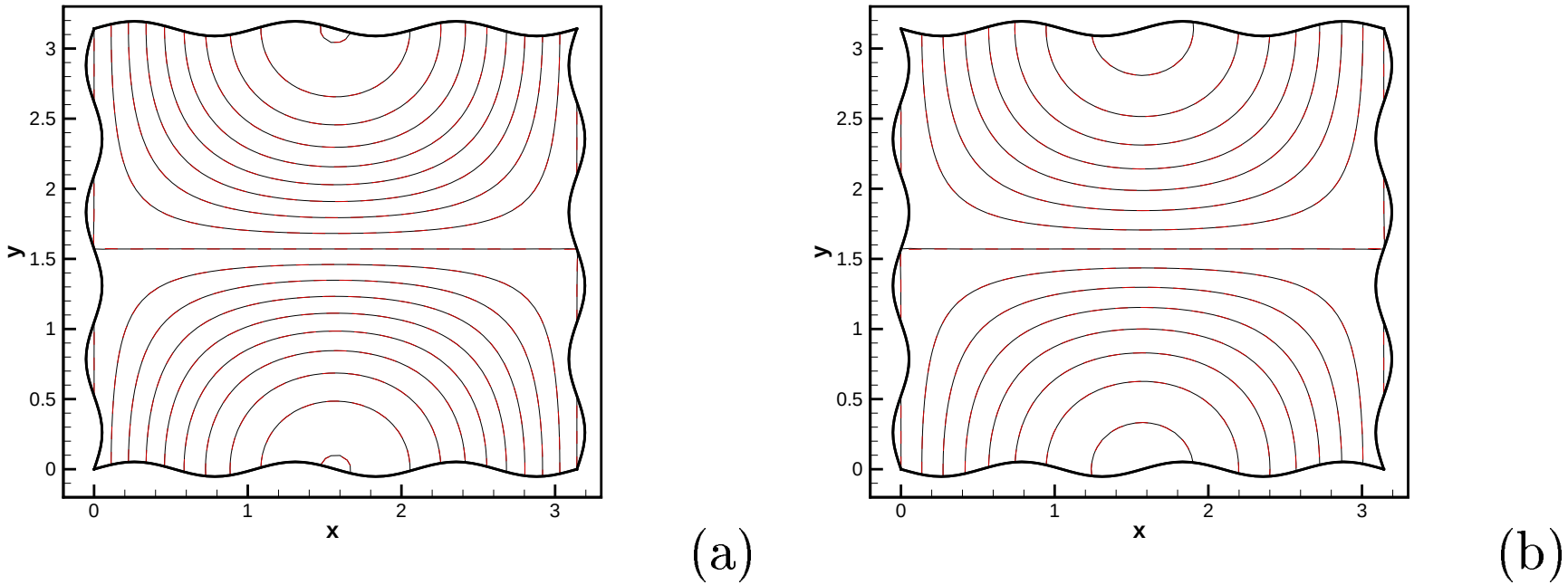

Figure 3: *Comparison of vertical velocity at time (a) $t = 5$, (b) $t = 15$.*

Flow Decayed by Viscosity

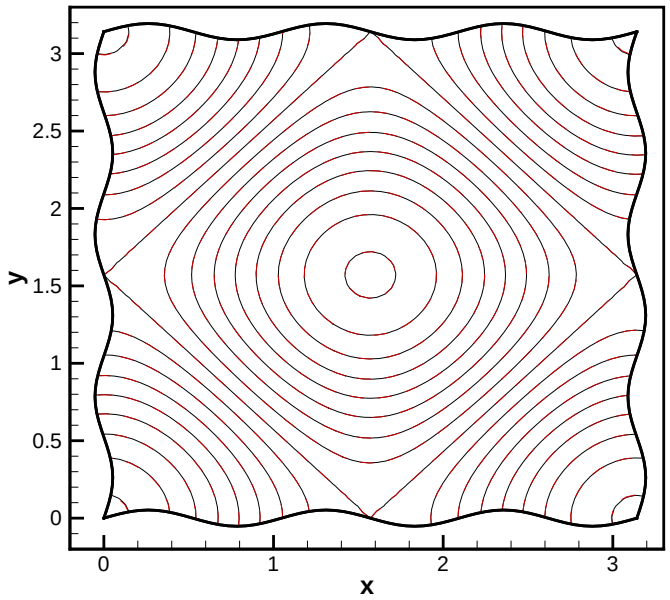

(a)

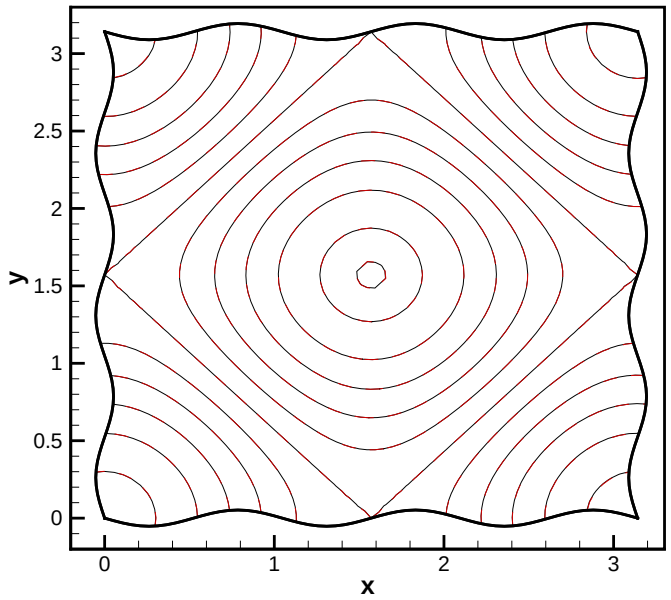

(b)

Figure 4: *Comparison of pressure at time (a) $t = 5$, (b) $t = 15$.*

Flow Decayed by Viscosity

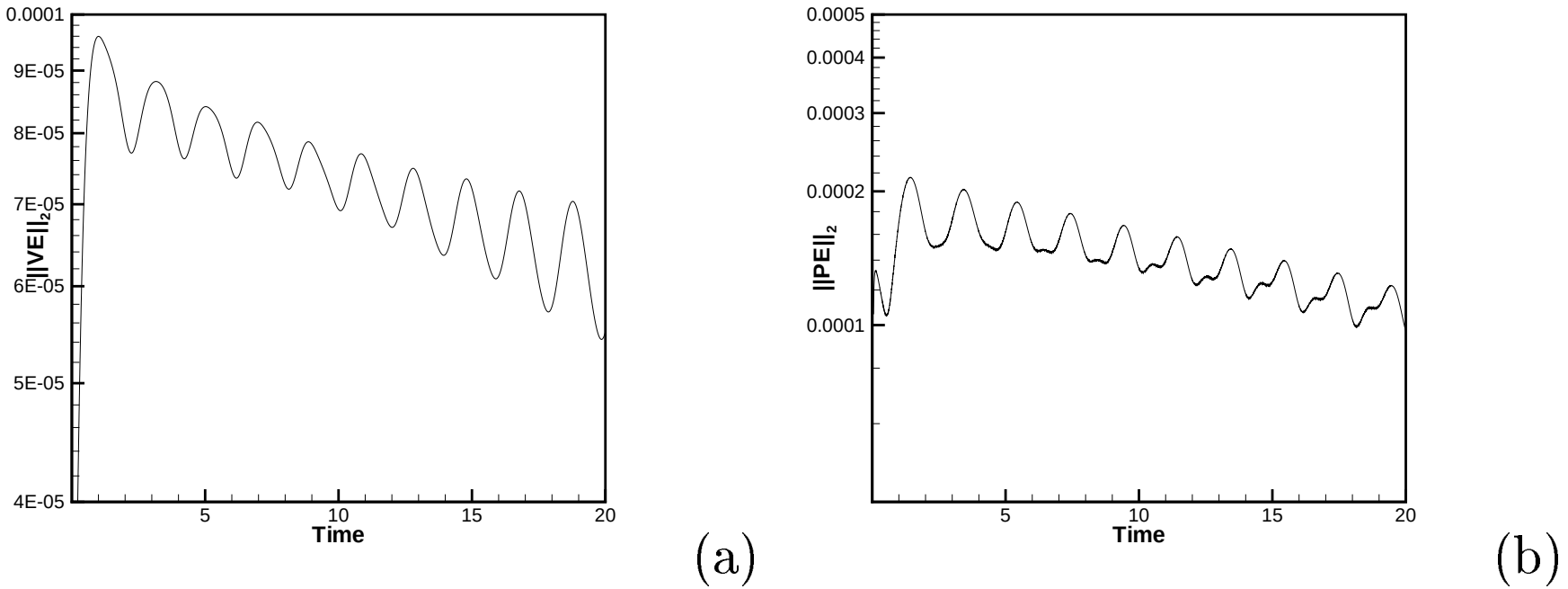

Figure 5: *Time history of error (a) horizontal velocity, (b) pressure.*

Freestream Preservation

Using the previous grid we examine freestream preservation property an uniform flow $(u, v) = (u_\infty, 0)$, computed using 2D N-S equations.

Boundary condition:

1. For horizontal velocity, $u_\infty = 1$ is imposed on left, top and bottom deforming boundaries. Downstream convective condition is used.
2. For vertical velocity, $v = 0$ is imposed on all sides.
3. Pressure on the boundaries is computed using

$$\hat{n}.\nabla p = \hat{n}.\left(\frac{1}{Re}\nabla^2\vec{q} - (\vec{q}.\nabla)\vec{q}\right).$$

Table 1: *Freestream Preservation Errors for 2D Wavy Mesh*

Scheme	Error $\|\|v\|\|_\infty$	Error $\|\|p\|\|_\infty$
With GCL	2×10^{-29}	1×10^{-29}
Without GCL	4×10^{-29}	4×10^{-29}

Lid-driven Cavity

We test by computing lid-Driven cavity flow using a time varying grid. The grid susceptible to extreme contraction and stretching is:

$$\begin{aligned} x &= \xi + 1500\xi^6(\xi - 1/2)(1-\xi)^6\eta(1-\eta)\sin(2\pi\tau), \\ y &= \eta + 1500\eta^6(\eta - 1/2)(1-\eta)^6\xi(1-\xi)\sin(2\pi\tau). \end{aligned} \tag{21}$$

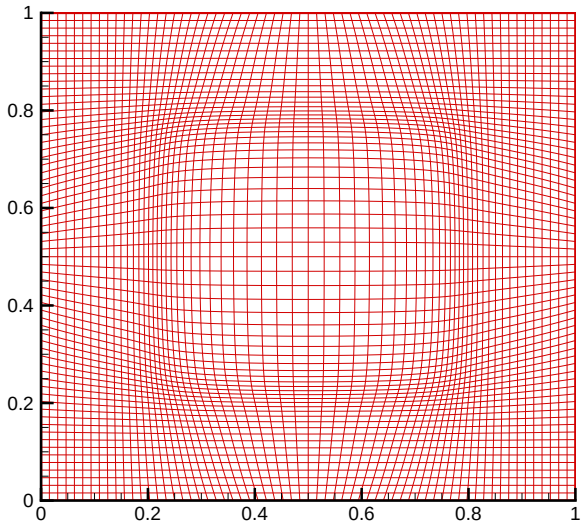

(a)

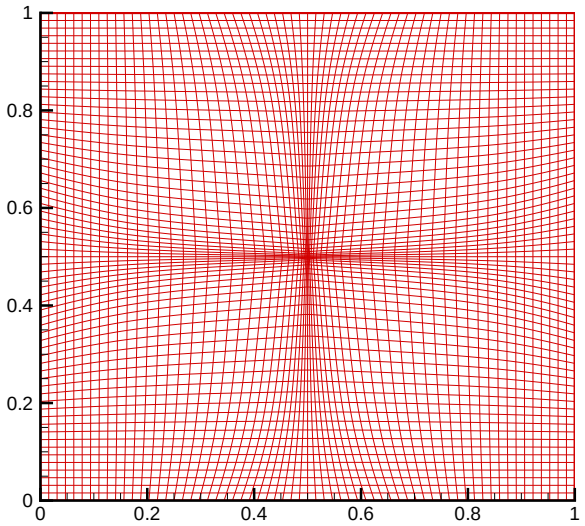

(b)

Figure 6: *Grid at time (a) $t = 0.25$, (b) $t = 0.75$.*

Lid-driven Cavity

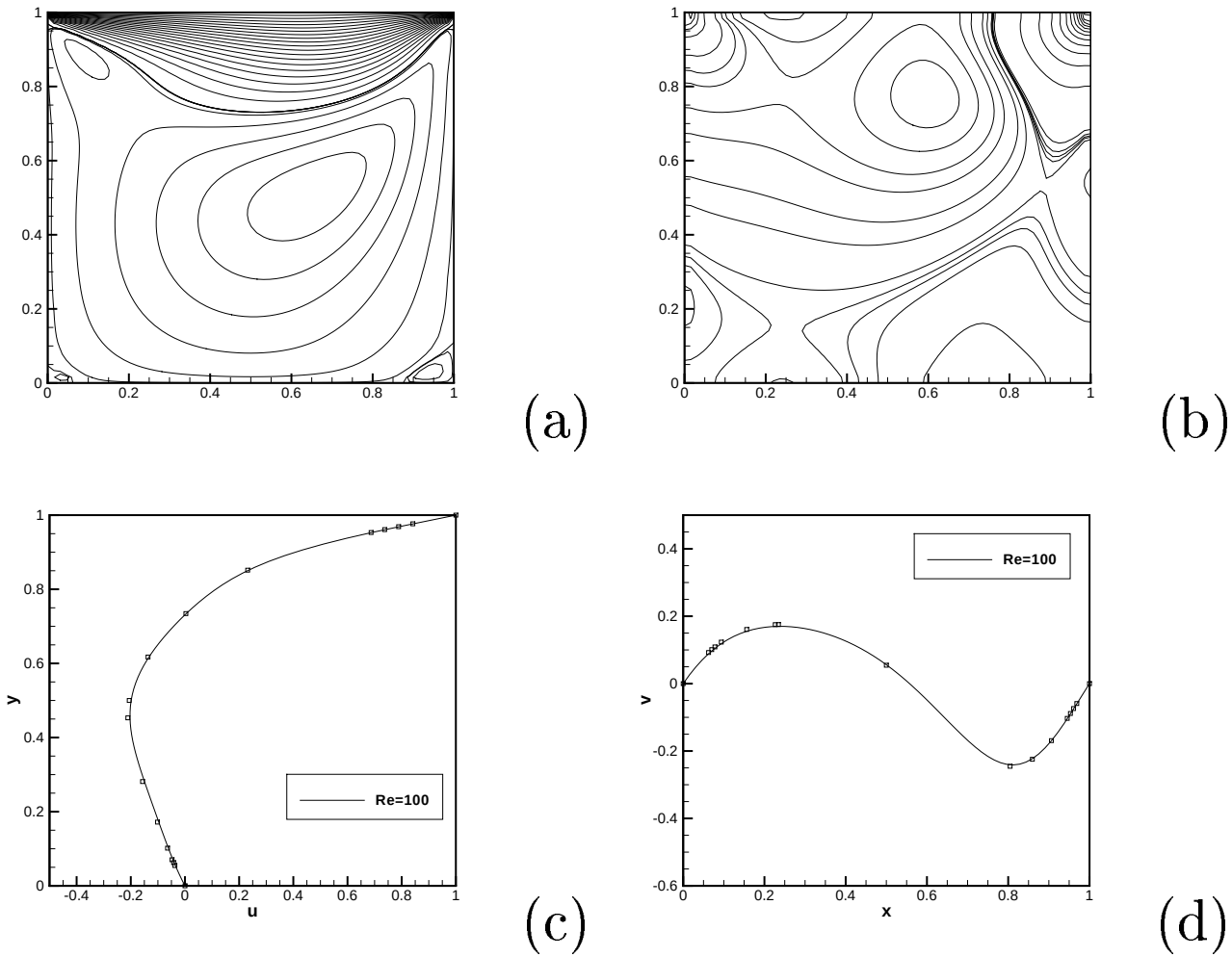

Figure 7: *(a) Horizontal velocity, (b) pressure, (c) u along vertical centreline and (d) v along horizontal centreline for $Re = 100$ (1982, [12]).*

Lid-driven flow in Deforming Cavity

The scheme is applied to a closed flow case with deforming boundary. Lower wall of the cavity deforms with a prescribed form [11] as:

$$y = A\sin(2\pi f\tau)\left(e^{c(\xi-a_1)^2} - e^{c(\xi-a_2)^2}\right) \tag{22}$$

with $A = 0.1,\ \ f = 0.2,\ \ c = 60,\ \ a_1 = 0.375,\ \ a_2 = 0.675,\ \ 0 < \xi \leq 1.$

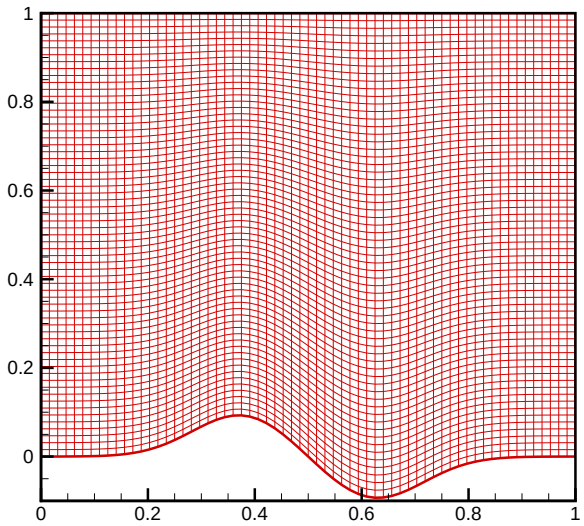

(a)

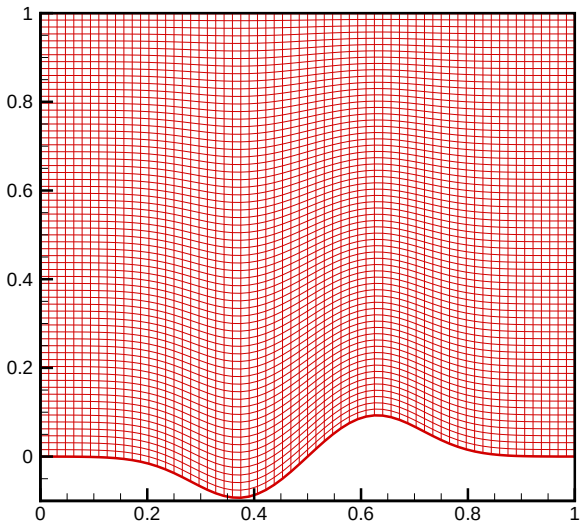

(b)

Figure 8: *Grid at time (a) $t = 1.0$, (b) $t = 4.0$.*

Lid-driven flow in Deforming Cavity

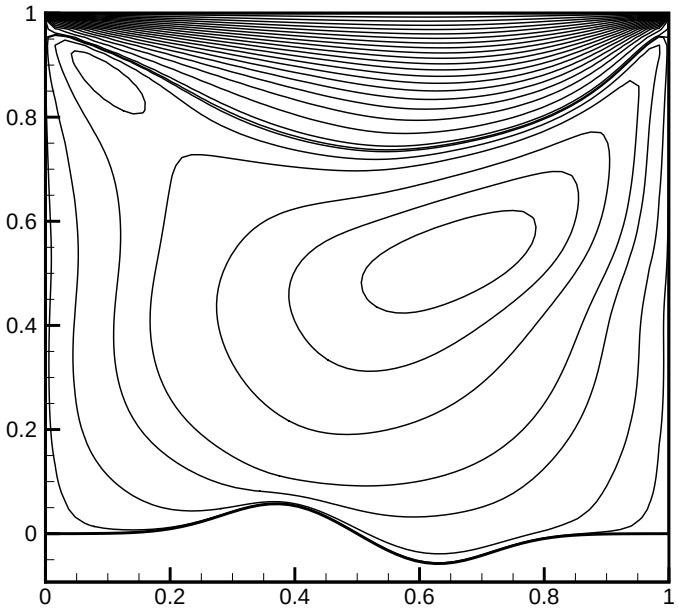

(a)

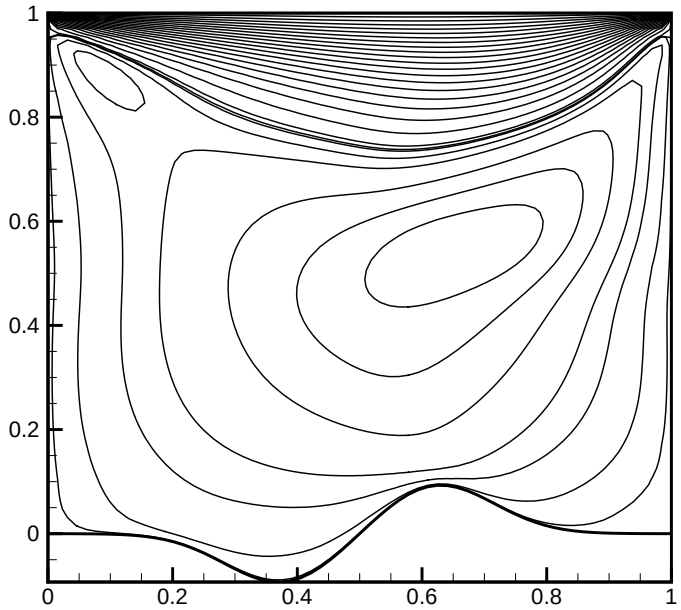

(b)

Figure 9: *Horizontal velocity at periodic state for* $Re = 100$.

Lid-driven flow in Deforming Cavity

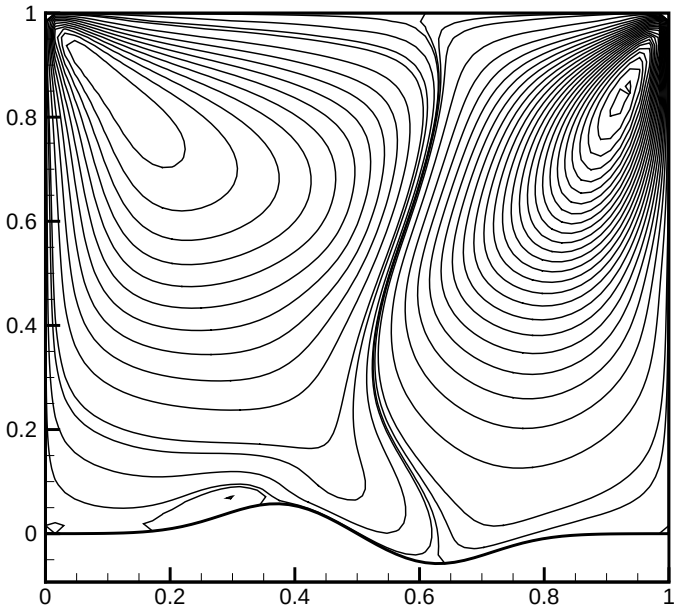

(a)

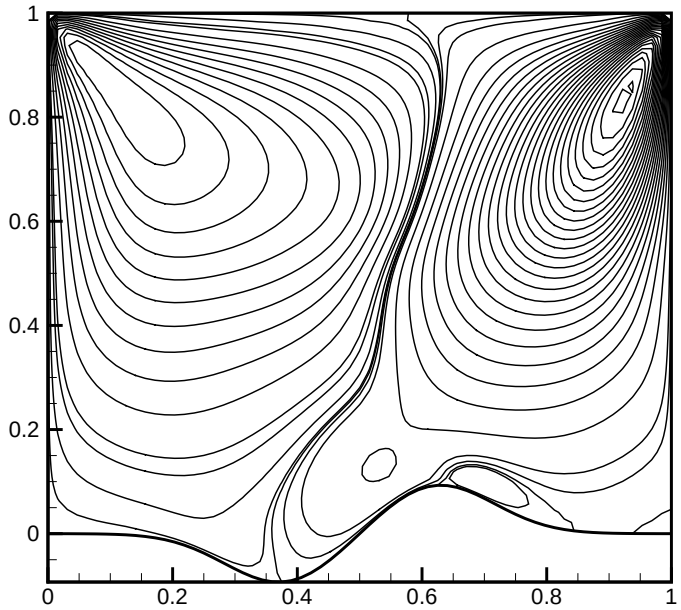

(b)

Figure 10: *Vertical velocity at periodic state for* $Re = 100$.

Lid-driven flow in Deforming Cavity

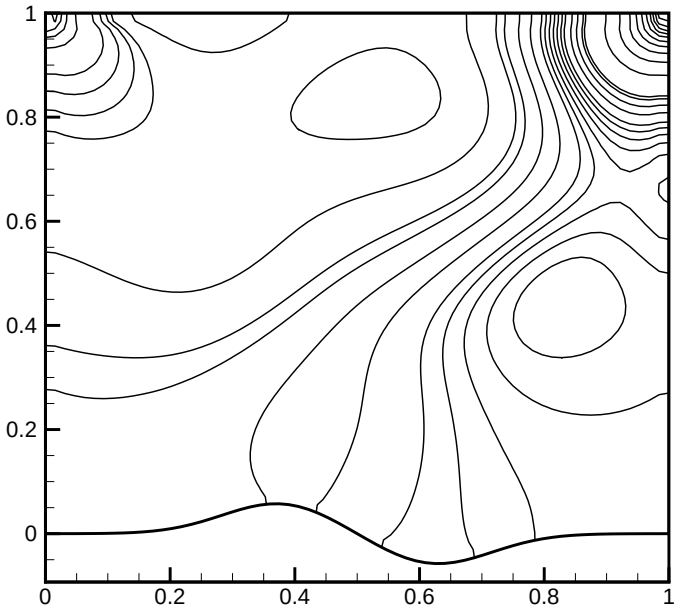

(a)

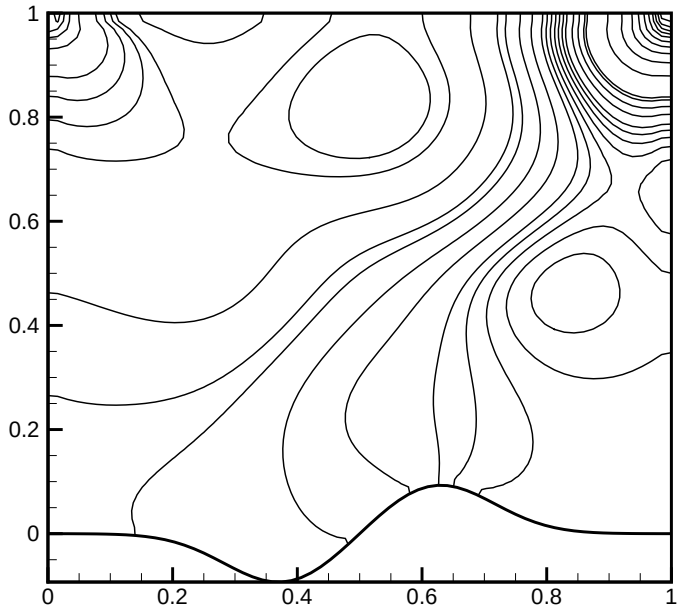

(b)

Figure 11: *Pressure contour at periodic state for* $Re = 100$.

Lid-driven flow in Deforming Cavity

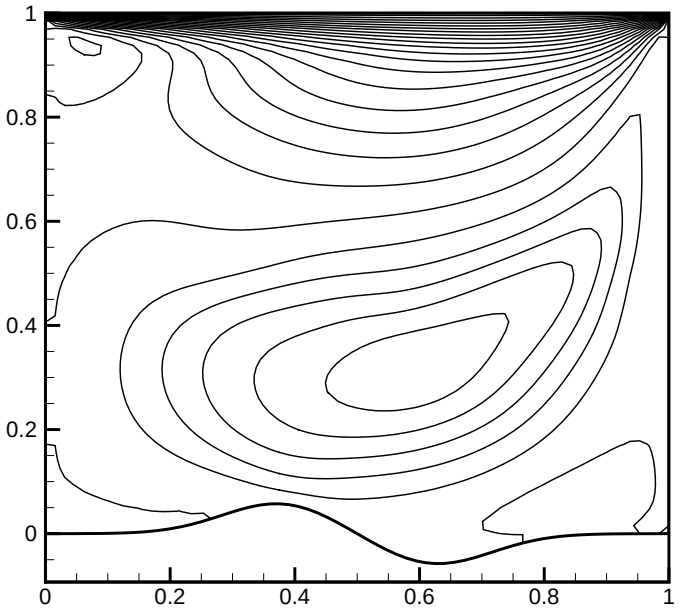

(a)

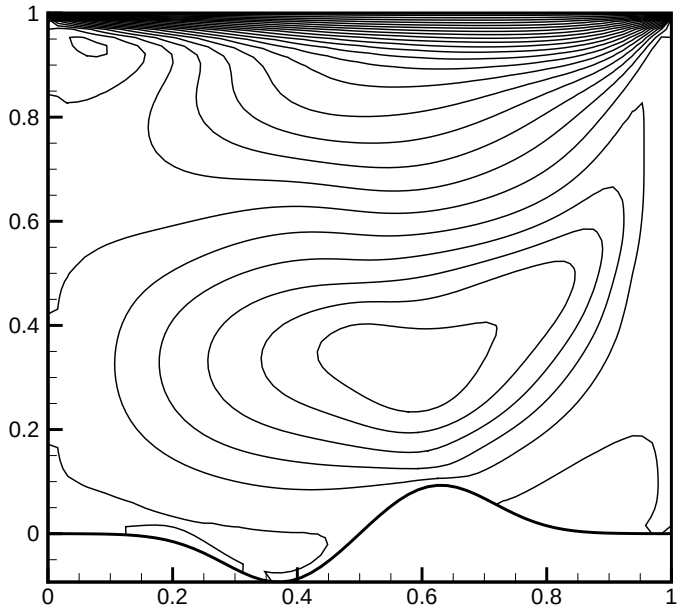

(b)

Figure 12: *Horizontal velocity at periodic state for* $Re = 500$.

Lid-driven flow in Deforming Cavity

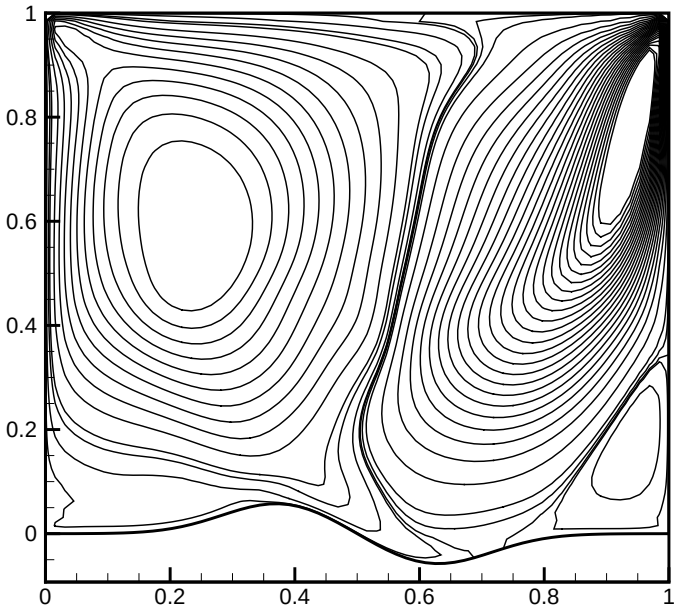

(a)

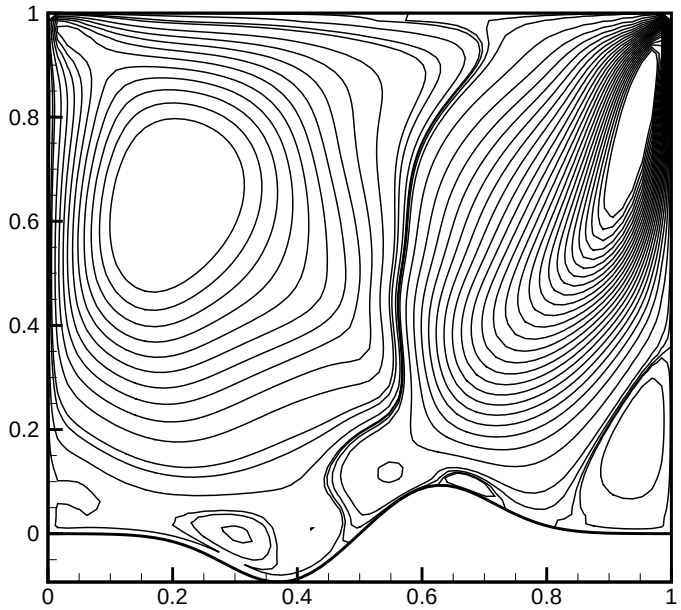

(b)

Figure 13: *Vertical velocity at periodic state for* $Re = 500$.

Lid-driven flow in Deforming Cavity

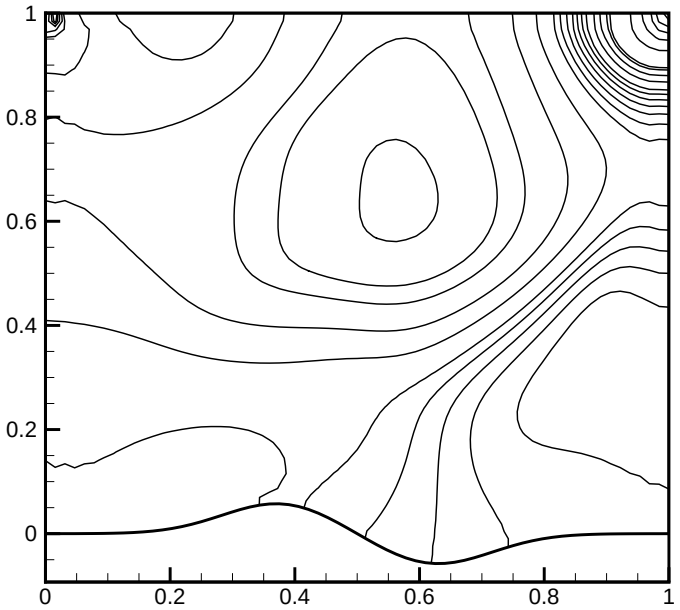

(a)

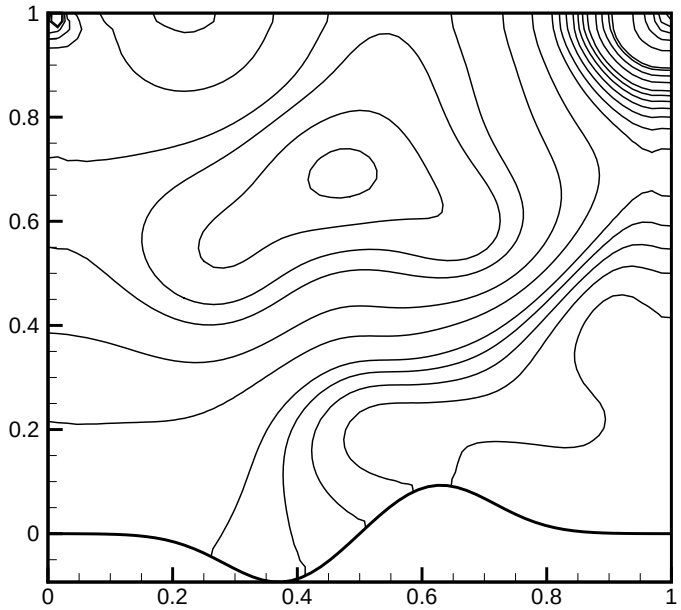

(b)

Figure 14: *Pressure contour at periodic state for* $Re = 500$.

Lid-driven flow in Deforming Cavity

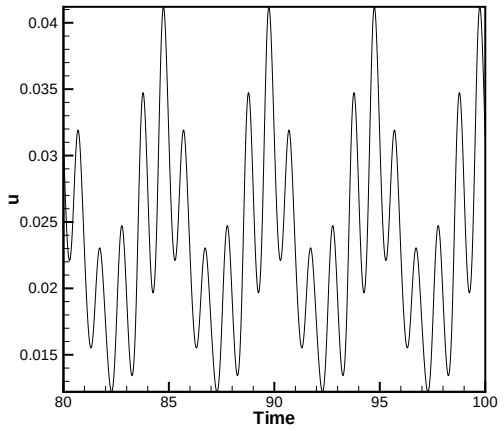

(a)

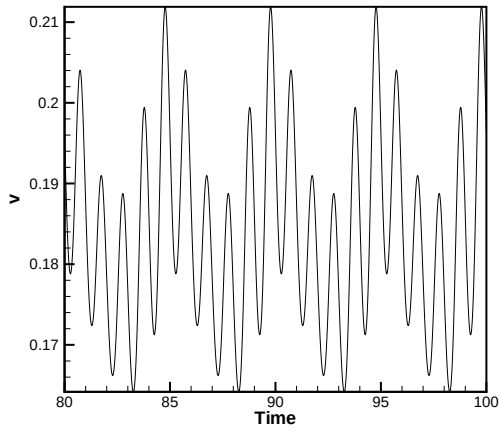

(b)

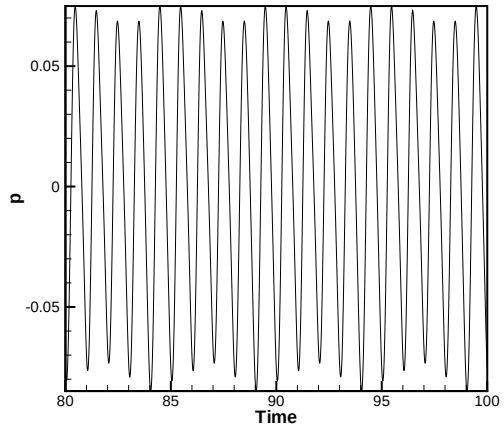

(c)

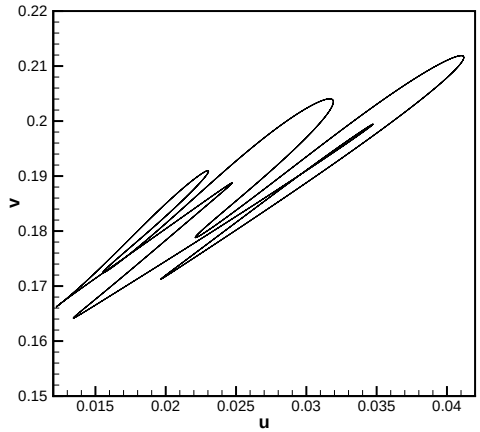

(d)

Figure 15: *(a) Horizontal velocity, (b) vertical velocity, (c) pressure history and (d) phase portrait of u versus v at (2/16, 13/16) for $Re = 500$.*

Oscillating cylinder in Cross-flow

Study the case of circular cylinder oscillating laterally in a free stream.

- Streamfunction vorticity formulation is used

$$\frac{\partial \omega}{\partial t} + u\omega_x + v\omega_y - \frac{1}{Re}(\omega_{xx} + \omega_{yy}) = 0$$
$$-(\psi_{xx} + \psi_{yy}) = \omega.$$

- Oscillatory velocity transverse to the flow is imposed

$$V_c = 2A_r \pi f_r \cos(2\pi f_r \tau), \quad f_r = f_n/f_c, \quad A_r = A_c/D.$$

- Numerically generated multi-block grid is used.
- IDW interpolation is used to generate time deforming grid.

Oscillating cylinder in Cross-flow

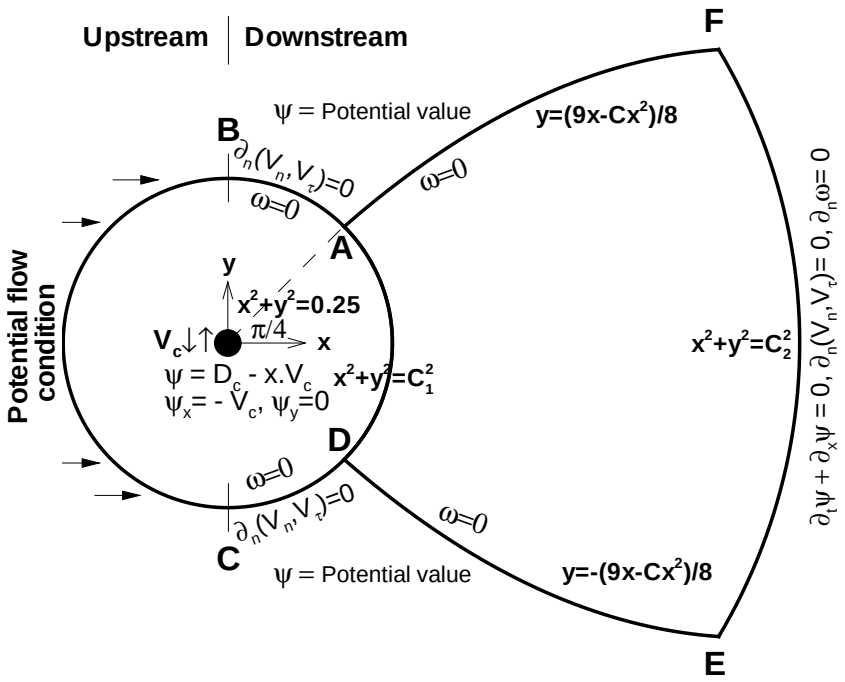

Figure 16: *Schematic diagram of cylinder oscillating in cross-flow.*

Oscillating cylinder in Cross-flow

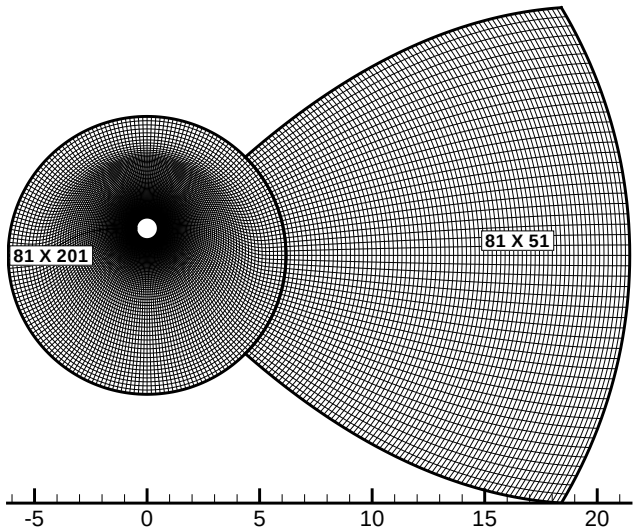

(a)

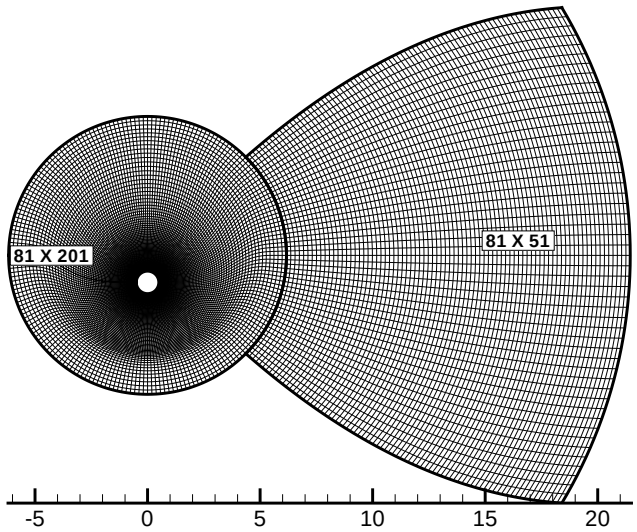

(b)

Figure 17: *Deformed grid using IDW at time (a)* $t = 2.0$, *(b)* $t = 6.0$ *with* $A_r = 1.2$, $f_r = 1.6$.

Oscillating cylinder in Cross-flow

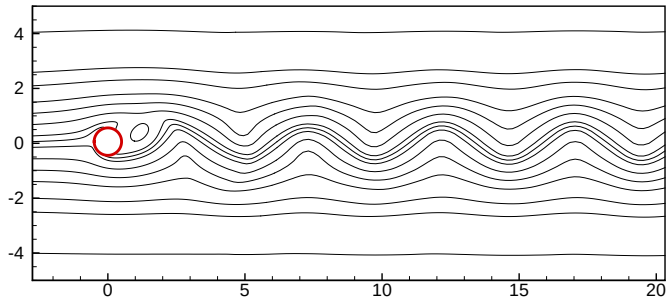

(a)

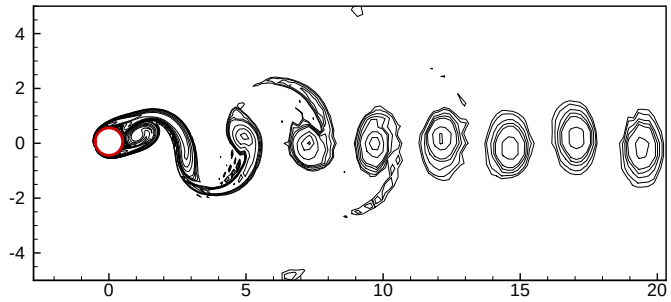

(b)

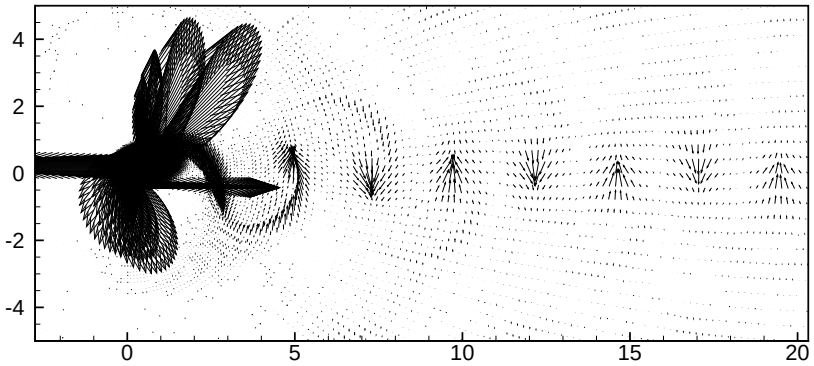

(c)

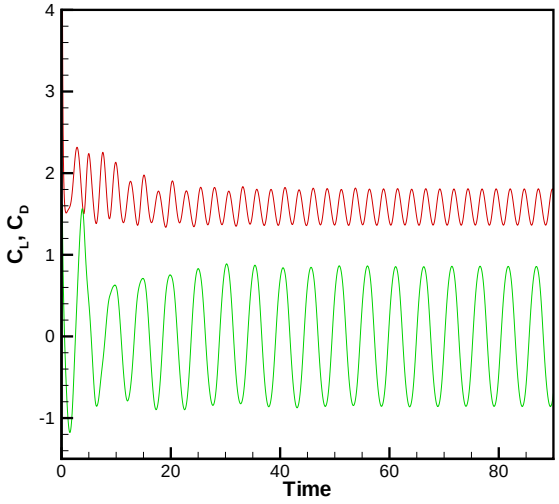

(d)

Figure 18: *(a) Streamlines, (b) Vorticity contours, (c) Lamb vector plot, (d) Drag and Lift coefficients at* $A_r = 0.4$, $f_r = 1.03$, $Re = 392$.

Oscillating cylinder in Cross-flow

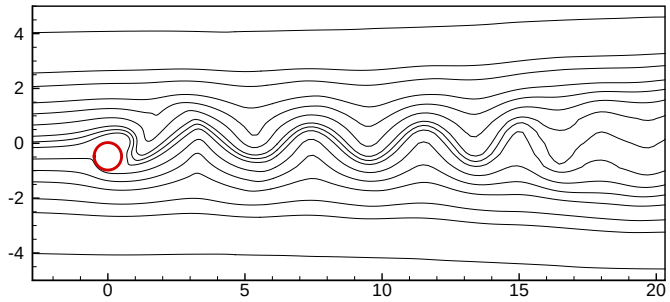

(a)

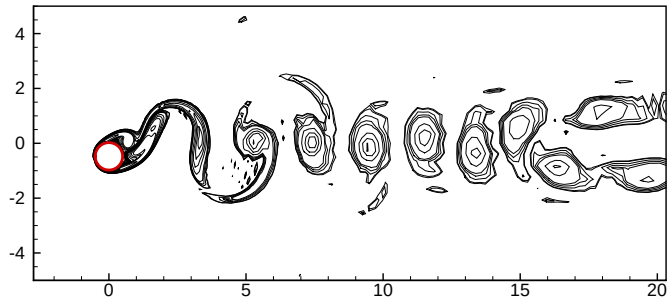

(b)

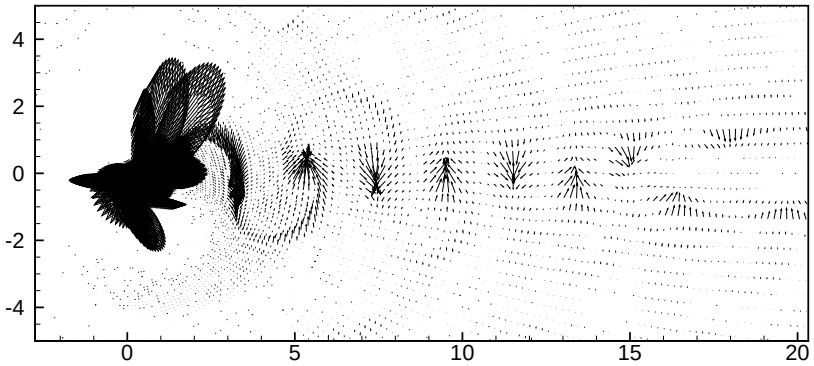

(c)

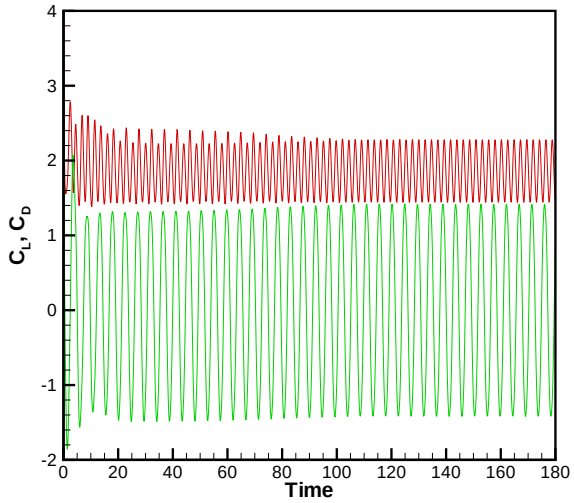

(d)

Figure 19: *(a) Streamlines, (b) Vorticity contours, (c) Lamb vector plot, (d) Drag and Lift coefficients at* $A_r = 0.5$, $f_r = 0.93$, $Re = 392$.

Oscillating cylinder in Cross-flow

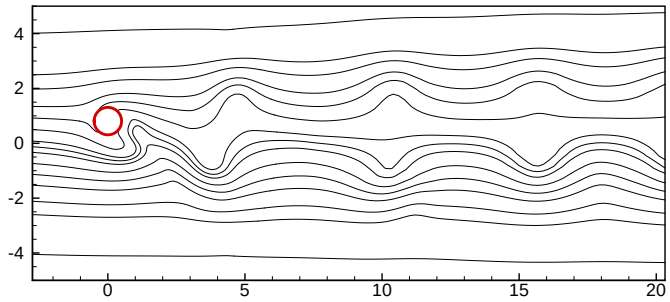

(a)

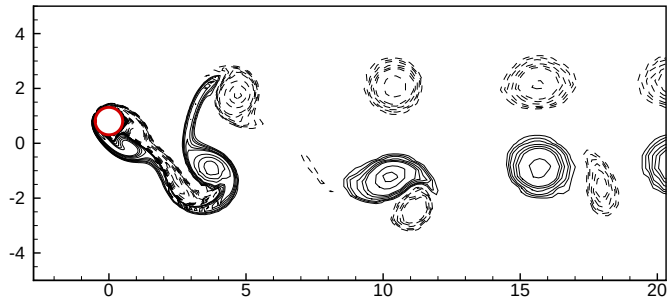

(b)

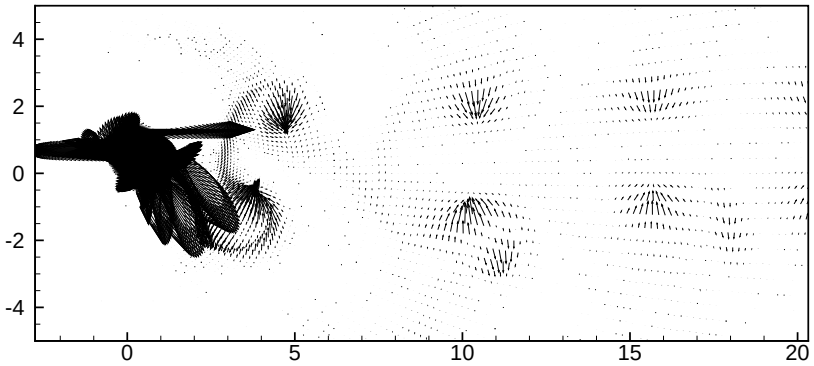

(c)

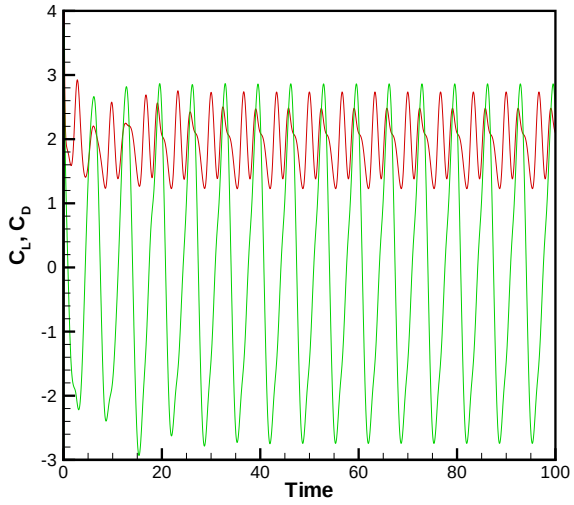

(d)

Figure 20: *(a) Streamlines, (b) Vorticity contours, (c) Lamb vector plot, (d) Drag and Lift coefficients at* $A_r = 1.0$, $f_r = 1.33$, $Re = 200$.

Oscillating cylinder in Cross-flow

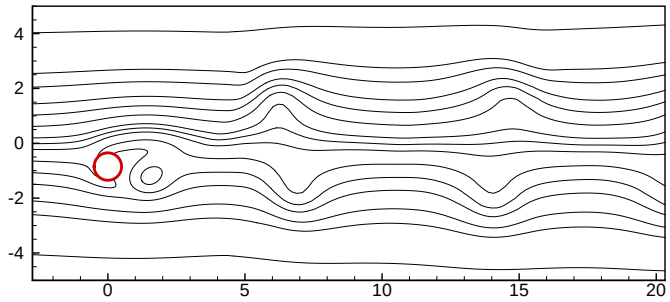

(a)

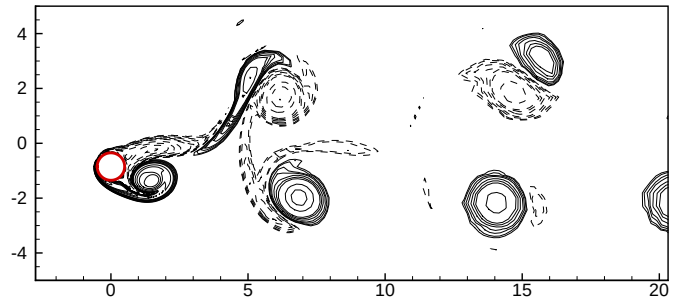

(b)

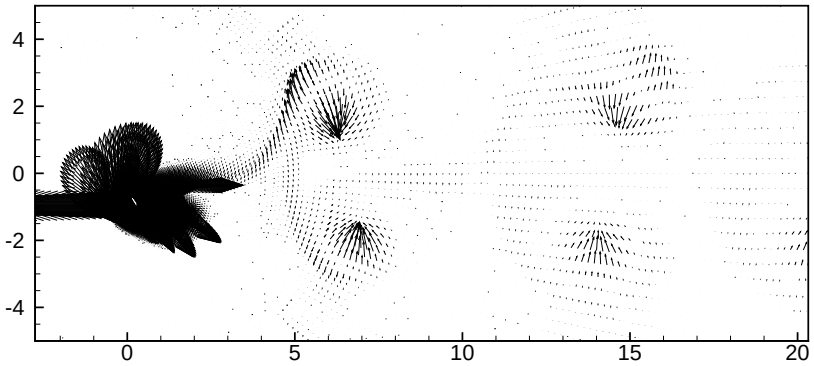

(c)

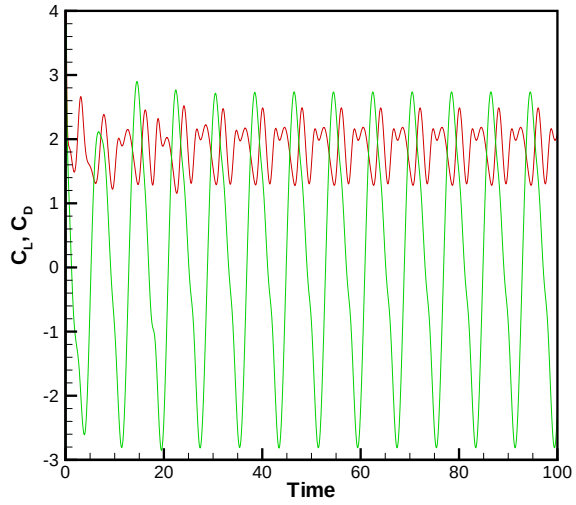

(d)

Figure 21: *(a) Streamlines, (b) Vorticity contours, (c) Lamb vector plot, (d) Drag and Lift coefficients at* $A_r = 1.2$, $f_r = 1.6$, $Re = 200$.

Oscillating cylinder in Cross-flow

(streamlines A=0.4 F=1.03 Re=392)

(vorticity A=0.4 F=1.03 Re=392)

(streamlines A=0.5 F=0.93 Re=392)

(vorticity A=0.5 F=0.93 Re=392)

(streamlines A=1.0 F=1.33 Re=200)

(vorticity A=1.0 F=1.33 Re=200)

(streamlines A=1.2 F=1.6 Re=200)

(streamlines A=1.2 F=1.6 Re=200)

Outline

References I

1. M. R. Visbal and D. V. Gaitonde, On the use of higher-order finite-difference schemes on curvilinear and deforming meshes, Journal of Computational Physics 181 (2002) 155-185.
2. S. Sen, A new family of (5,5) CC-4OC schemes applicable for unsteady Navier-Stokes equations, Journal of Computational Physics 251 (2013) 251-271.
3. S. Sen, Fourth order compact schemes for variable coefficient parabolic problems with mixed derivatives, Computers and Fluids 134-135 (2016) 81-89.
4. P. D. Thomas, C. K. Lombard, Geometric conservation law and its application to flow computations on moving grids, AIAA Journal 17 (1979) 1030-1037.
5. K. Ou, (2012) High-order methods for unsteady flows on unstructured dynamic meshes, Ph.D. Thesis, Stanford University.
6. Y. Abe, N. Iizuka, T. Nonomura, K. Fujii, Conservative metric evaluation for high-order finite difference schemes with the GCL identities on moving and deforming grids, Journal of Computational Physics 39 (1981) 201-255.
7. Y. Abe, T. Haga, T. Nonomura, K. Fujii, Conservative high-order flux-reconstruction schemes on moving and deforming grids, Computers and Fluids 139 (2016) 2-16.
8. J. A. S. Witteveen, H. Bijl, Explicit mesh deformation using inverse distance weighting interpolation. 19th AIAA Computational Fluid Dynamics Conference, AIAA, San Antonio, Texas, AIAA Paper, 3996, 2009.

References II

9. J. A. S. Witteveen, Explicit and robust inverse distance weighting mesh deformation for CFD. 48th AIAA Aerospace Sciences Meeting Including the New Horizons Forum and Aerospace Exposition, Orlando, Florida, AIAA Paper, Vol. 165, 2010.

10. E. Luke, E. Collins, E. Blades, A fast mesh deformation method using explicit interpolation. Journal of Computational Physics, 231 (2012) 586-601.

11. Y. Chen, X. Xie, Vorticity vector-potential method for 3D viscous incompressible flows in time-dependent curvilinear coordinates, Journal of Computational Physics, 312 (2016) 50-81.

12. U. Ghia, K. N. Ghia, C. T. Shin, High-Re solutions for incompressible flow using the Navier-Stokes equations and a multigrid method, Journal of Computational Physics 48 (1982) 387-411.

Thank you for your attention.